

Numerical Modeling of Brain Dynamics in Traumatic Situations - Impulsive Translations

Martin Burtscher

School of Electrical and Computer
Engineering, Cornell University
Ithaca, NY 14853, U.S.A.

Igor Szczyrba

Department of Mathematical Sciences
University of Northern Colorado
Greeley, CO 80639, U.S.A.

Abstract *We numerically model the brain dynamics during and after impulsive head translations using linear Partial Differential Equations (PDEs) describing viscoelastic solids and a nonlinear generalization of these PDEs describing incompressible, viscoelastic fluids. The brain matter motion and the sensitivity of the solutions with respect to the skull's geometry differ substantially in the two cases. In particular, the oscillatory rotational flows, which we discovered to appear in the matter after the translations stop, are quite distinct. The significance of the results for understanding the mechanisms of Closed Head Injuries (CHI) is discussed.*

Keywords: Linear and nonlinear CHI dynamics.

1 Introduction

The most successful model of CHI to date emphasizes the role of shear waves in the injury creation. The initial version of this model [1] uses the linear, partial differential Voigt¹ equations describing viscoelastic solids:

$$\frac{\partial \mathbf{v}}{\partial t} = \Delta(c^2 \mathbf{u} + \nu \mathbf{v}), \quad \frac{\partial \mathbf{u}}{\partial t} = \mathbf{v}, \quad \nabla \cdot \mathbf{u} = 0. \quad (1)$$

Here, $\mathbf{v}(\mathbf{x}, t)$ is the time-dependent, spatial velocity vector field, $\mathbf{u}(\mathbf{x}, t)$ is the corresponding displacement vector field, $c \equiv \sqrt{G/\delta}$ is the velocity of the shear waves (where G is the shear

¹System (1) is also referred to as Kelvin-Voigt [2], Kelvin [3], or Navier-Stokes equations [4]. We omit Kelvin's name since it should be used when an additional term is present [5]. We invoke Navier-Stokes' name when the full material derivative is involved.

modulus and δ is the density of the medium), and ν denotes the kinematic viscosity coefficient. The analytic solutions of (1) found in [4] for impulsive head rotations explained the mechanism of bridging-vein hematomas and lead to establishing brain injury tolerance criteria for Diffuse Axonal Injuries (DAI) [2]. However, these equations cannot explain why DAI are scattered in a pointwise manner in the white matter, predominantly along its boundaries with the gray matter or ventricles [6, 7].

In our research on impulsive head rotations about the brain's 'center' [8, 9, 10], we have been able to recreate these subtle features of DAI using a nonlinear generalization of system (1). Our approach treats the brain tissue as a viscoelastic, incompressible fluid (the human brain contains 78% water)². Specifically, we augment the standard Navier-Stokes equations with a term that describes elastic media, i.e., we model the brain's dynamics in traumatic scenarios by means of the following PDEs:

$$\begin{aligned} \frac{D\mathbf{v}}{Dt} &= -\nabla \tilde{p} + \Delta(c^2 \mathbf{u} + \nu \mathbf{v}), \\ \frac{D\mathbf{u}}{Dt} &= \mathbf{v}, \quad \nabla \cdot \mathbf{v} = 0, \end{aligned} \quad (2)$$

where $D/Dt \equiv \partial/\partial t + (\mathbf{v} \cdot \nabla)$ denotes the material derivative, and $\tilde{p}(\mathbf{x}, t)$ is the (normalized by δ) sum of the standard pressure and the hydrostatic compression of solids [8].

Head rotations have been the primary focus of CHI research since it has been argued

²The need to replace (1) by equations that account for the brain's fluidity is widely accepted, cf., e.g., [3].

that translations should have a negligible impact on CHI [1, 11] due to the brain’s incompressibility. This argument sounds reasonable for steady translations, but an abrupt stop or change of direction may lead to a traumatic rotational movement within the tissue. In fact, substantial brain injuries appear among boxers and shaken babies despite minimal rotations of their heads. Modeling head translations also helps understand the brain dynamics during head rotations about an arbitrary axis, e.g., about the neck. Such a rotation can be approximated by a sequence of small rotations about the head’s ‘center’ alternated with small translations in varying directions.

Analytic solutions of (1) are only known for a cylinder and a sphere rotated about the center [4], whereas analytic solutions of (2) are not even known for such basic scenarios. For an impulsive translation of a skull containing an incompressible medium, the initial boundary condition (that the skull is moved in a fixed direction) violates the requirement $\nabla \cdot \mathbf{v} = 0$. Thus, proving the existence of analytic solutions in this case is far more complicated than for rotations and most likely requires the use of perturbation methods [12]. As of now, numerical approaches are the only way to study the solutions of (1) and (2) in realistic scenarios.

A new version of our finite difference numerical solver, which has been validated against the known analytic solutions of (1), allows us to model the brain dynamics during and after impulsive translations of an impenetrable skull (whose ‘interaction’ with the outside environment is suppressed). Our previous simulations of impulsive head rotations about the ‘center’ [13] imply that the skull’s geometry is an important factor in determining the brain motion in traumatic scenarios. Therefore, besides simulating translations of realistic 2D brain cross-sections, we also simulate identical motions of a variety of idealized cross-sections with circular, elliptic, rectangular, etc., boundaries. A comparison of the results reveals important differences between the linear and nonlinear cases and thus helps us understand the role of the brain’s fluidity in CHI creation.

2 Simulation Setup

To clearly separate the dynamic consequences of translations from other factors (e.g., the differences in physical properties between the gray and the white matter, cf. [8, 9]), we treat the brain tissue as a uniform mixture of the gray and the white matter with the shear wave velocity $c=1.5\text{m/s}$, viscosity $\nu=0.01\text{m}^2/\text{s}$, and density $\delta=1.06 \times 10^3 \text{kg/m}^3$. These physical properties imply the length of the shortest shear waves that can propagate in the tissue to be *circa* 0.02m [8]. To properly model such short waves and maintain good numerical stability of the solutions, a grid resolution of $1 \cdot 10^{-3}\text{m} \leq \Delta x \leq 2 \cdot 10^{-3}\text{m}$ and a time step of $2 \cdot 10^{-5}\text{s} \leq \Delta t \leq 1 \cdot 10^{-4}\text{s}$ is used.

We assume there is no slippage between the skull and the brain, i.e., for all (idealized and realistic) brain cross-sections, the boundary between the brain and the skull reflects the shape of the brain. We use analytic formulas for circular, elliptic, rectangular, etc., boundaries whereas for realistic sagittal and horizontal cross-sections, we introduce (based on medical data) spline approximations of the brain’s shape. The *falx cerebri* is modeled as a solid substructure rigidly attached to the skull.

We impulsively translate brain cross-sections for up to 0.05s with the velocity $V=1\text{m/s}$. We chose V to be significantly smaller than c to prevent nonlinear effects from leading to an excessive turbulent flow that would overshadow the basic rotational features of the solutions, see [9, 10, 13]. The relatively short translation times are selected because our model, as well as the Voigt model, assumes a linear relation between strain and stress, which is only appropriate when small displacements are created. To deal with large deformations, nonlinear relations should be used [14]. Since the analytic solutions of (1) [4] as well as our theoretical and numerical results [8] imply that the shear waves are damped exponentially, we monitor the solutions for only up to 0.3s. Thus, each simulation requires up to 15,000 time steps with up to 40,000 nodes being calculated in each time step.

3 Results

In the following, we refer to simulations based on linear system (1) and nonlinear system (2) as **L** and **NL**, respectively. The solutions presented are obtained for translations lasting $T=0.05\text{s}$, but their qualitative features are also representative for shorter translations. The results are shown in the coordinate system attached to the skull. The vector magnitudes in the vector field plots are scaled down to make the plots ‘readable’. The 3D graphs representing vector components depict true values. All translations are horizontal from left to right.

A **NL** translation of a circular cross-section of radius 0.08m leads to a piling up of the brain tissue on the left side where it is pushed, as the several right-pointing displacement vectors $\mathbf{u}=(u_x, u_y)$ with $u_x > 0$ in Fig. 1 show. These positive values of u_x increase in time, but the region they appear in remains limited to a narrow strip on the left. The remaining vectors with $u_x < 0$ reflect that the brain matter lags behind in the cross-section.

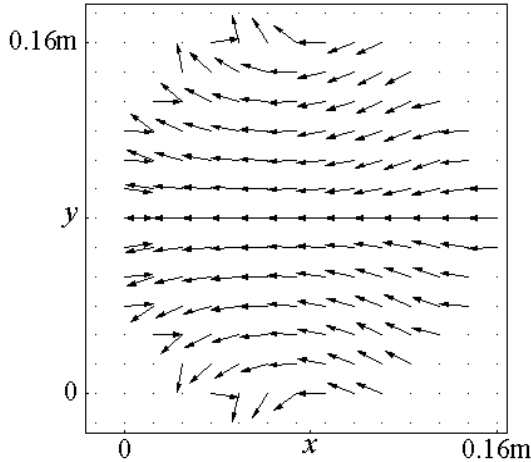


Fig. 1: Circular cross-section - **NL**.

The displacement field $\mathbf{u}(x, y)$ at $t = 0.03\text{s}$.

In the **L** case, no piling up takes place and the lagging is the largest in the middle of the cross-section, Fig. 2. Contrary to analytic [4] and our previous results concerning rotations³,

³Constant rotations lead to a periodic, tangential lagging/outpacing and the creation of shear waves by both systems. For a tangential $V=1\text{m/s}$ and c, ν as above, the maximum lagging appears in a circle at $t \approx 0.03\text{s}$. Then the process of outpacing begins [4, 8].

no outpacing happens during constant translations in either case. However, nonzero values of u_y appear due to the incompressibility condition $\nabla \cdot \mathbf{v} = 0$. The maxima (minima) depicted in Fig. 3 for the **NL** case correspond to the localized upward (downward) flow, and are also representative of the **L** case.

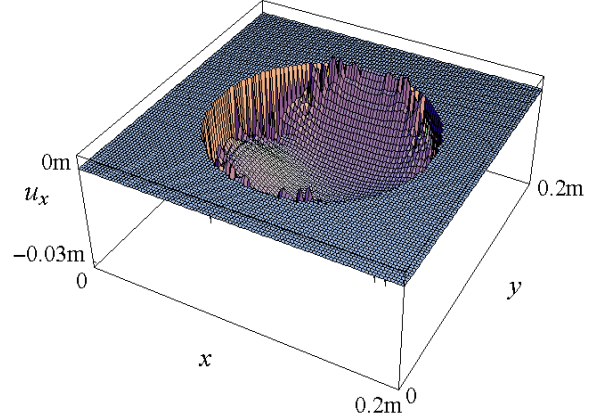


Fig. 2: Circular cross-section - **L**.
The $u_x(x, y)$ component at $t = 0.03\text{s}$.

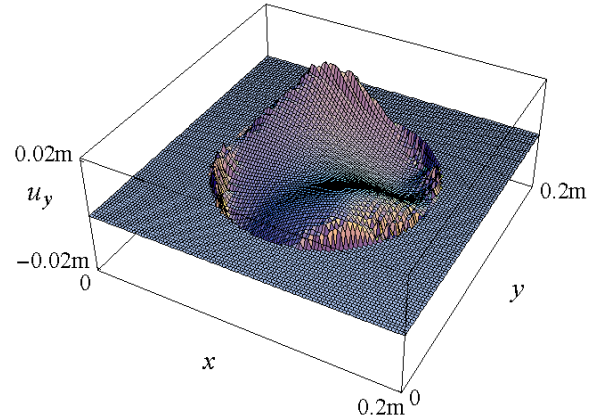


Fig. 3: Circular cross-section - **NL**.
The $u_y(x, y)$ component at $t = 0.03\text{s}$.

The corresponding velocity vector fields $\mathbf{v}=(v_x, v_y)$ are also predominantly horizontal during translations in both cases (the graphs of \mathbf{v} , v_x and v_y mimic Figs. 1, 2 and 3). In the **L** case, $|v_x| \leq V=1\text{m/s}$, whereas the maximum $v_y \approx 0.5\text{m/s}$. Our simulations with various idealized and realistic cross-sections imply that during translations the skull’s shape is largely irrelevant to the general features of the solutions presented above. This concerns also the turbulent flow that appears in the **NL** case in two localized regions to the left where

$|v_x|$ substantially exceeds V , Figs. 4 and 5.⁴

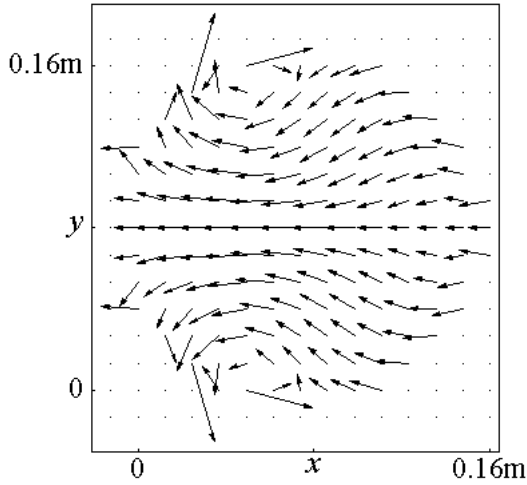


Fig. 4: Circular cross-section - **NL**.
The velocity field $\mathbf{v}(x, y)$ at $t = 0.04s$.

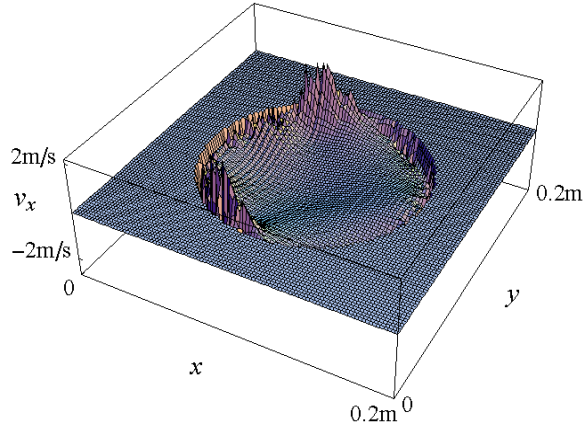


Fig. 5: Circular cross-section - **NL**.
The $v_x(x, y)$ component at $t = 0.04s$.

When the forcing stops in the circular **L** case, two vortices form rotating the matter in opposite directions, Fig. 6. The rotations reverse after just 0.015s, Fig. 7, and the oscillations continue with a frequency of *circa* 0.035s, going through patterns of six, four, or just two vortices, cf. Footnote 3. The values of the component v_x before the first reversal are depicted in Fig. 8, 0.0025s after the translation, i.e., at the time when the induced material velocity has already been halved (the graph of v_y mimics Fig. 3, with the maximum $v_y \approx 0.25m/s$).

⁴A similar local magnification of the material velocity occurs in rotations of noncircular brain cross-sections [13]. Once the material velocity exceeds the velocity c of the shear waves, a turbulent flow usually appears leading to large displacements [8].

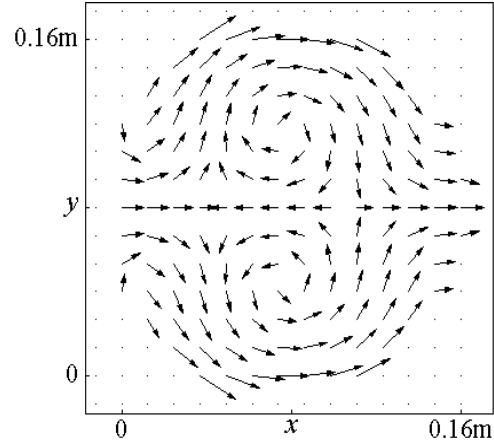


Fig. 6: Circular cross-section - **L**.
The velocity field $\mathbf{v}(x, y)$ at $t = 0.0501s$.

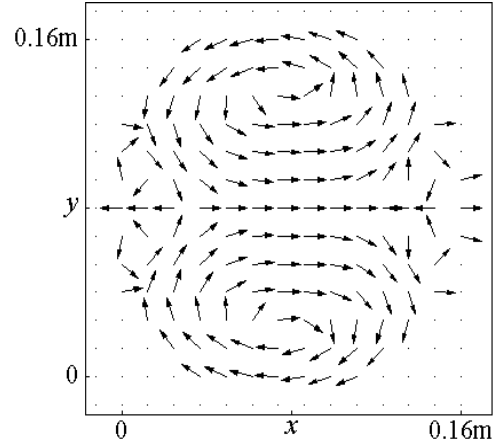


Fig. 7: Circular cross-section - **L**.
The velocity field $\mathbf{v}(x, y)$ at $t = 0.065s$.

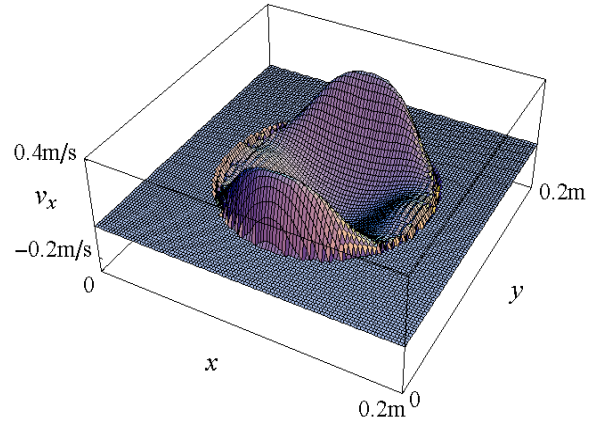


Fig. 8: Circular cross-section - **L**.
The $v_x(x, y)$ component at $t = 0.0525s$.

If the width exceeds the height of the cross-section, e.g., as is the case in a sagittal cross-section of a human brain, the velocity field in the **L** case also forms two well-defined vortices,

Figs. 9 and 10. The brightest spots depict the maximum velocity $v_x \approx 1\text{m/s}$.

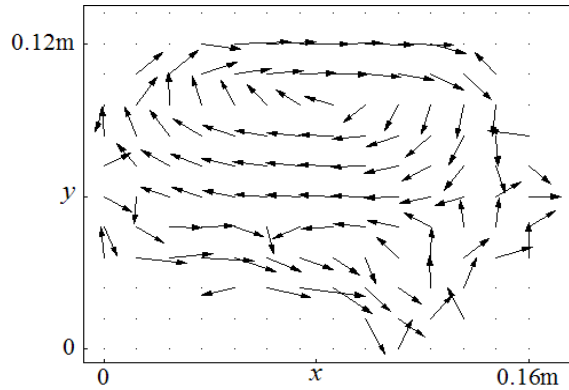


Fig. 9: Sagittal cross-section - **L**.
The velocity field $\mathbf{v}(x, y)$ at $t = 0.0501\text{s}$.

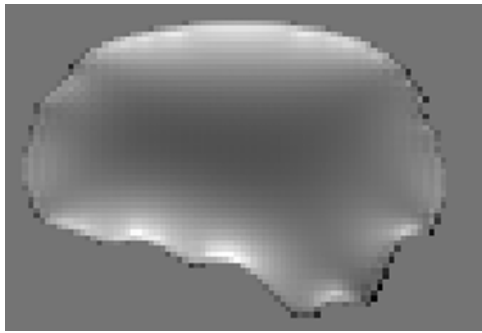


Fig. 10: Sagittal cross-section - **L**.
The $v_x(x, y)$ component at $t = 0.0501\text{s}$.

In a horizontal brain cross-section whose height exceeds its width, six vortices are created, Fig. 11. They periodically merge and reappear, going through complicated oscillatory patterns of five, four, three, or just two vortices.

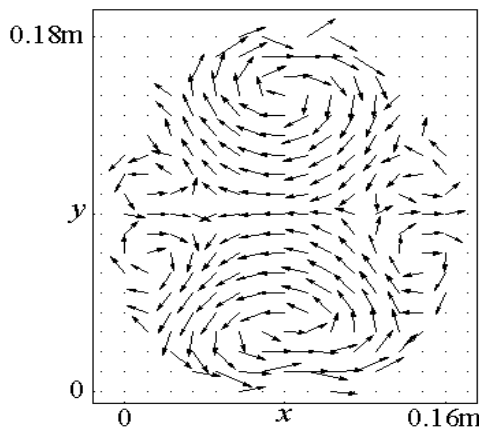


Fig. 11: Horizontal cross-section
without *falx cerebri* - **L**.
The velocity field $\mathbf{v}(x, y)$ at $t = 0.0501\text{s}$.

The NL system creates quite different solutions after the forcing has stopped. Indeed, four vortices tend to form regardless of the shape, Figs. 12, 13 and 14.

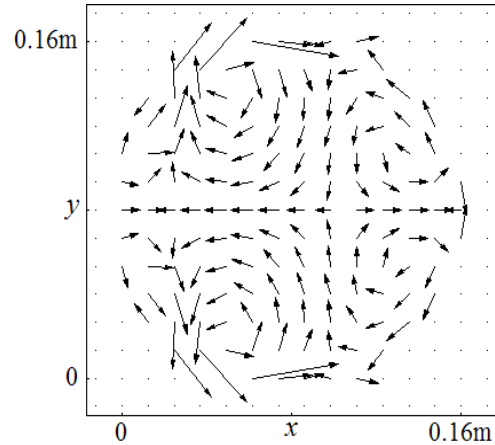


Fig. 12: Circular cross-section - **NL**.
The velocity field $\mathbf{v}(x, y)$ at $t = 0.0501\text{s}$.

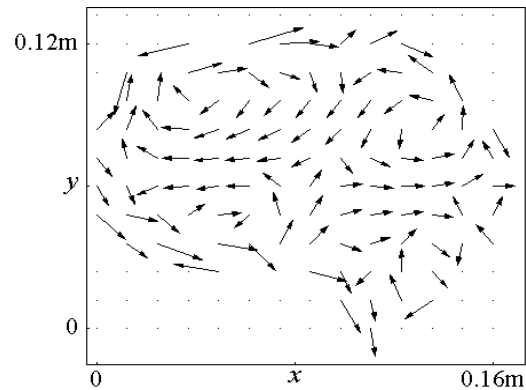


Fig. 13: Sagittal cross-section **NL**.
The velocity field $\mathbf{v}(x, y)$ at $t = 0.0501\text{s}$.

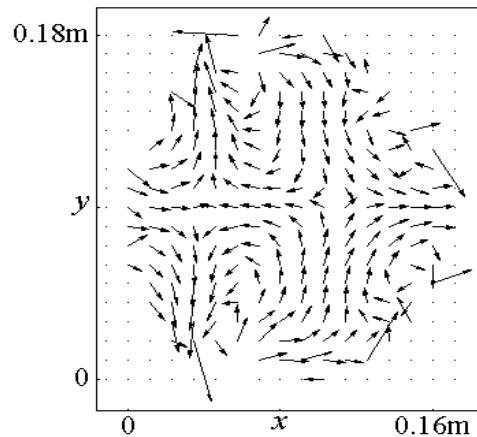


Fig. 14: Horizontal cross-section
without *falx cerebri* - **NL**.
The velocity field $\mathbf{v}(x, y)$ at $t = 0.0501\text{s}$.

Vectors not in unison with the rotations appear due to the turbulent flow, cf. Fig. 5. Since in the realistic cases the vortices are not as well-defined as in the circle, the rotational motions become more ‘disorganized’ with time (but the oscillatory patterns are similar to the **L** case).

For the horizontal cross-section with *falx cerebri* fully separating the hemispheres, the **L** case leads to eight vortices, Fig. 15, whereas the analogous **NL** case only results in four vortices, Fig. 16.

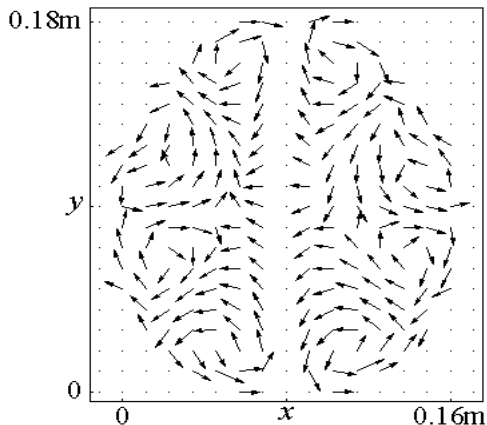


Fig. 15: Horizontal cross-section with *falx cerebri* - **L**.

The velocity field $\mathbf{v}(x, y)$ at $t = 0.0501\text{s}$.

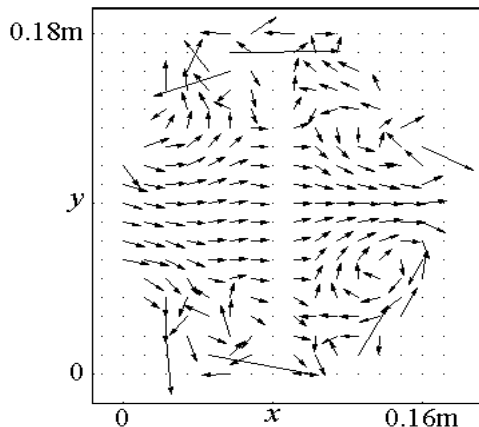


Fig. 16: Horizontal cross-section with *falx cerebri* - **NL**.

The velocity field $\mathbf{v}(x, y)$ at $t = 0.0501\text{s}$.

In fact, the latter solution resembles more the four-vortex **NL** solution obtained without *falx cerebri*, cf. Fig. 14, than the solution depicted in Fig. 15.⁵ This is because in the **NL** case,

⁵A similar result has been observed during rotations of these two types of cross-sections [13].

the maxima of $v_x \approx 2\text{m/s}$ are assumed at the same two locations, Fig. 17, as they are in the connected domain, cf. Fig. 5, and the turbulent flow appearing in both types of domains overshadows the influence of topology.

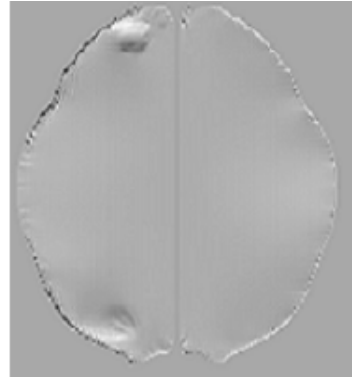


Fig. 17: Horizontal cross-section with *falx cerebri* - **NL**.

The $v_x(x, y)$ component at $t = 0.0501\text{s}$.

The oscillatory patterns in the disconnected domains are similar to those in the connected cross-sections. However, in the **L** case with a disconnected domain, the v_x decrease is twice as large 0.0025s after the translation, Fig. 18, as it is in the connected case, cf. Fig. 8.

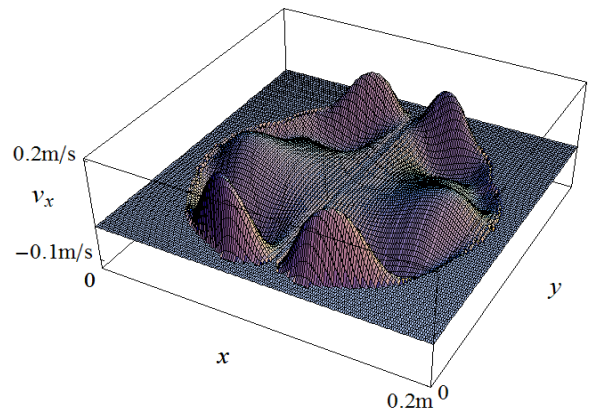


Fig. 18: Horizontal cross-section with *falx cerebri* - **L**.

The $v_x(x, y)$ component at $t = 0.0525\text{s}$.

4 Conclusions

A general similarity of the solutions of both PDE systems consists of a lagging of the brain matter during the translation and of a complicated rotational motion afterwards. A piling up of the brain matter and a significant, lo-

calized increase of the material velocity resulting in a turbulent flow during and after translations is characteristic only for the nonlinear system (2). Because of this flow, the character of the rotational motion (e.g., number of vortices) created by (2) does not depend as much on the shape and the topology of the cross-sections as it does with the linear system (1). The solutions of system (2) are more influenced by the shape and the topology as far as their time evolution is concerned whereas system (1) leads to more persistent rotational patterns.

The discovered rotational patterns can help understand CHI mechanisms, e.g., why even an abrupt, short head translation may create injuries in specific localizations (cf. contracoup injuries) as well as what role the brain's fluidity plays in this respect. Moreover, during repetitive translations the subsequent impulsive translations face quite different initial conditions since the first interrupted translation already results in a rotational movement. Thus, more and more damaging rotations can arise, especially if a resonance occurs. Investigating such scenarios could shed light on the mechanisms of the shaken baby syndrome.

References

- [1] A. H. S. Holbourn. Mechanics of head injury. *Lancet*, 2:438-441, 1943.
- [2] S. Margulies and L. Thibault. A Proposed Tolerance Criterion for Diffuse Axonal Injury in Man. *J. Biomech.*, 25:917-923, 1992.
- [3] Q. Zhu and J. K. F. Suh. Dynamic Biphasic Poroviscoelastic Model Simulation of Hydrated Soft Tissues and Its Potential Applications for Brain Impact Study. *Proc. Bioeng. Conf.*, AMSE BED 50:835-836, 2001.
- [4] C. Ljung. A Model for Brain Deformation Due to Rotation of the Skull. *J. Biomech.*, 8:263-274, 1975.
- [5] Y. C. Fung. "Biomechanics: Mechanical Properties of Living Tissues", 2nd ed, 41-42, Springer Verlag, 1993.
- [6] W. Maxwell, J. Povlishock and D. Graham. A Mechanistic Analysis of Nondisruptive Axonal Injury: A Review. *J. Neurotrauma*, 14:419-440, 1997.
- [7] P. Leclercq, J. Mckenzie, D. Graham and S. Gentleman. Axonal Injury is Accentuated in the Caudal Corpus Callosum of Head-Injured Patients. *J. Neurotrauma*, 18:1-10, 2001.
- [8] C. S. Cotter, P. K. Smolarkiewicz and I. N. Szczyrba, A Nonlinear Model for Brain Injuries. *Proc. METMBS'00*, 2:443-449, CSREA Press, 2000.
On Mechanisms of Diffuse Axonal Injuries. *Proc. Bioeng. Conf.*, AMSE BED 50:315-317, 2001.
A Viscoelastic Model for Brain Injuries. *Int. J. for Numerical Methods in Fluids*, 40:303-311, 2002.
- [9] I. N. Szczyrba, P. K. Smolarkiewicz and C. S. Cotter, Numerical Simulations of Closed Head Injuries, *Proc. METMBS'02*, 2:486-492, CSREA Press, 2002.
- [10] I. Szczyrba and M. Burtscher, On the Role of Ventricles in Diffuse Axonal Injuries, *Proc. Bioeng. Conf.*, Key Biscayne FL, 147-148, 2003, <http://hopper.unco.edu/faculty/personal/szczyrba/publications.htm>
- [11] I. M. Thomas, Mechanism of Head Injury, in "Impact Injury and Crash Protection", Ch. 2:27-42, Thomas Books, 1969.
- [12] C. S. Morawetz, The Mathematical Approach to the Sonic Barrier, *Bulletin (New Series) of the American Mathematical Society*, Vol. 6, No. 2:127-145.
- [13] M. Burtscher and I. Szczyrba, On the Role of the Brain's Geometry in Closed Head Injuries, to appear in the *Proc. Bioeng. Conf.*, Vail CO, June 2005,
- [14] E. Takhounts, J. Crandall and K. Darvish, On the Importance of Nonlinearity of Brain Tissue Under Large Deformations, *Sapp Car Crash J.*, 47:79-92, 2003.